

AD-A150 988

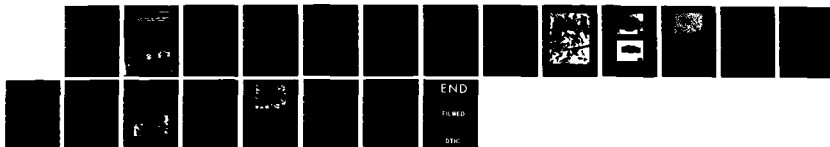
LOCALIZED CORROSION CURRENTS FROM GRAPHITE/ALUMINUM AND
WELDED SiC/AL METAL MATRIX COMPOSITES(U) NAVAL RESEARCH
LAB WASHINGTON DC C R CROWE 28 FEB 85 NRL-MR-5415

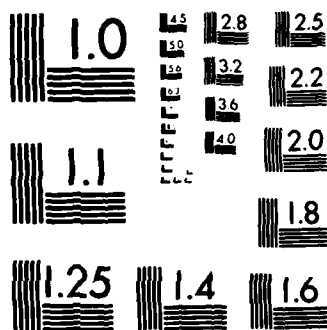
1/1

UNCLASSIFIED

F/G 11/6

NL





MICROCOPY RESOLUTION TEST CHART
NATIONAL BUREAU OF STANDARDS 1963-A

AD-A150 988

ORIGINAL FILE COPY

Localized Cervical
and Thoracic

TRAVELER'S COMPASS

REPORT DOCUMENTATION PAGE

1a REPORT SECURITY CLASSIFICATION UNCLASSIFIED				1b RESTRICTIVE MARKINGS			
2a SECURITY CLASSIFICATION AUTHORITY				3 DISTRIBUTION/AVAILABILITY OF REPORT Approved for public release; distribution unlimited.			
2b DECLASSIFICATION/DOWNGRADING SCHEDULE							
4 PERFORMING ORGANIZATION REPORT NUMBER(S) NRL Memorandum Report 5415				5 MONITORING ORGANIZATION REPORT NUMBER(S)			
6a NAME OF PERFORMING ORGANIZATION Naval Research Laboratory		6b OFFICE SYMBOL (if applicable) Code 6370		7a NAME OF MONITORING ORGANIZATION Defense Advanced Research Projects Agency			
6c ADDRESS (City, State, and ZIP Code) Washington, DC 20375-5000				7b ADDRESS (City, State, and ZIP Code) Arlington, VA 22209			
8a NAME OF FUNDING/SPONSORING ORGANIZATION DARPA		8b OFFICE SYMBOL (if applicable)		9 PROCUREMENT INSTRUMENT IDENTIFICATION NUMBER			
8c ADDRESS (City, State, and ZIP Code) Arlington, VA 22209				10 SOURCE OF FUNDING NUMBERS			
PROGRAM ELEMENT NO 62712E		PROJECT NO 4Y10		TASK NO. 4991		WORK UNIT ACCESSION NO. DN680-683	
11 TITLE (Include Security Classification) Localized Corrosion Currents from Graphite/Aluminum and Welded SiC/Al Metal Matrix Composites							
12 PERSONAL AUTHOR(S) Crowe, C.R.							
13a TYPE OF REPORT Progress		13b TIME COVERED FROM 11/83 TO 7/84		14 DATE OF REPORT (Year, Month, Day) 1985 February 28		15 PAGE COUNT 20	
16 SUPPLEMENTARY NOTATION <i>Cont'd</i>							
17 COSATI CODES			18 SUBJECT TERMS (Continue on reverse if necessary and identify by block number)				
FIELD	GROUP	SUB-GROUP	Corrosion, Electrochemistry Galvanic couple				
19 ABSTRACT (Continue on reverse if necessary and identify by block number) <i>Micro - FeT3 - SiC/Al</i> Scanning vibrating electrode techniques (SVET) have been used to study corrosion in Gr/Al and SiC/Al metal matrix composites. This new technique uses vibrating probes to measure localized ionic currents with spatial and current resolutions on the order of 15 to 20 μm and 5nA/cm ² , respectively. Thus, it is now possible to measure corrosion currents resulting from individual local cell activity on a scale closely related to many microstructural features of the composites. The relative severity of pits and crevices associated with the corrosion process. The observations demonstrate that corrosion effects from metallurgical variations due to welding to SiC/Al can be detected and areas of accelerated corrosion activity delineated. The observations of the corroding Gr/Al specimen imply that the corrosion rate of the composite in the absence of flaws would depend upon the catalytic properties of the graphite in promoting or retarding the oxygen reduction reaction as well as the rate (Continues)							
20 DISTRIBUTION/AVAILABILITY OF ABSTRACT <input checked="" type="checkbox"/> UNCLASSIFIED/UNLIMITED <input type="checkbox"/> SAME AS RPT <input type="checkbox"/> DTIC USERS				21 ABSTRACT SECURITY CLASSIFICATION UNCLASSIFIED			
22a NAME OF RESPONSIBLE INDIVIDUAL C. R. Crowe				22b TELEPHONE (Include Area Code) (202) 767-3433		22c OFFICE SYMBOL Code 6372	

19. ABSTRACT (Continues)

of diffusion of O_2 to the surface. Both the exchange current density for the reaction and the Tafel constant would affect the oxygen reduction reaction rate. Thus, the corrosion rate in the absence of flaws might be improved by additions of poisons to the fiber to retard the oxygen reduction reaction on graphite. The fact that an increase in the anodic current streaming from the flaws was detected indicates that the interface and crevice corrosion is important. Al_4C_3 formation at the Gr/Al interfaces and also the crevice corrosion characteristics of the aluminum matrix alloy may affect the degradation rate of the Gr/Al due to the exfoliation process. Selection of alloys for composite fabrication which are less susceptible to crevice corrosion and to Al_4C_3 formation during consolidation of the composite are likely to produce decreased rates. Improvements in transverse strength should also reduce exfoliation.

1. Limit of Supplied Requirements - 100%

100% (Block 18)

CONTENTS

INTRODUCTION	1
EXPERIMENTAL	3
Materials	3
Electrochemical Measurements	3
Scanning Electron Microscopy	6
RESULTS AND DISCUSSION	6
CONCLUSIONS	14
ACKNOWLEDGMENTS	14
REFERENCES	15

Accession For	
NTIS GRA&I	<input checked="" type="checkbox"/>
DTIC TAB	<input type="checkbox"/>
Unannounced	<input type="checkbox"/>
Justification	
By _____	
Distribution/	
Availability Codes	
Dist	Avail and/or Special
A-1	



LOCALIZED CORROSION CURRENTS FROM GRAPHITE/ALUMINUM AND WELDED SiC/Al METAL MATRIX COMPOSITES

INTRODUCTION

Recent advances in techniques of measuring localized currents in solutions have made possible methods to measure ionic currents associated with corrosion microcells. Basically, the new techniques use vibrating probes to measure localized ionic currents with spatial and current resolutions on the order of 15 to 20 μm and 5nA/cm², respectively. Thus, it is now possible to measure corrosion currents resulting from individual local cell activity on a scale closely related to many microstructural features of materials. This is particularly useful for studies of localized corrosion phenomena such as pitting and crevice corrosion and in studies of corrosion in composite materials where local galvanic effects between constituents and interfaces may be important.

Historically, the vibrating probe techniques were developed for biological studies¹⁻³ but have recently been used to study corrosion phenomena.⁴ Jaffe and his co-workers¹ developed a one-dimensional vibrating microprobe that demonstrated the methodology. The microprobe operates by oscillating a single electrode along a line and measuring the time-varying potential of the electrode relative to a fixed, distant reference electrode. The vibrating electrode is usually a small metal sphere 10 μm to 30 μm in diameter which is vibrated between two points typically 10 μm to 30 μm apart. The voltage at the two extremes of vibration is measured and used to calculate the current density component in the medium at the center of and along the axis of vibration by the relation

$$i \text{ (A/cm}^2\text{)} = \sigma \text{ (}\Omega\cdot\text{cm)}^{-1} \Delta V \text{ (volts)}/\Delta r \text{ (cm)} \quad (1)$$

where i is current density component parallel to probe vibration, ΔV is the voltage difference between the extremes of vibration, Δr is the vibration stroke, and σ is the conductivity of the solution.

The corrosion current density component normal to the surface or the net ion flux crossing the volume of material sampled by the probe at any specific region can be directly measured by vibrating the probe normal to the corroding surface just outside the corrosion cell. The local corrosion current density is then obtained by adjusting for the field fall-off between the surface and the center of probe vibration using an extrapolation procedure.

The electrode achieves high sensitivity by setting the oscillation at a frequency, f , where the $1/f$ noise is negligible. The basic principle is shown schematically in Fig. 1. A lock-in amplifier is used to restrict the

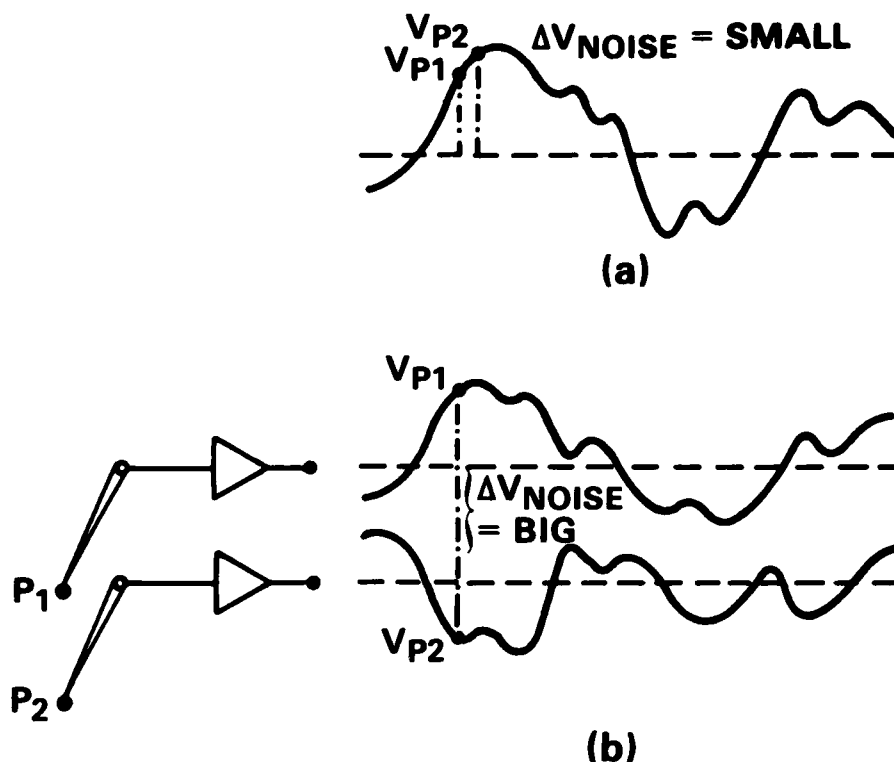


Fig. 1 - A schematic representation of the reduction of noise obtained by rapid oscillation of the electrode as compared to a slower, manual movement of the electrode between two points. (After Freeman, et al²)

measuring bandwidth to a small range of frequencies centered about the oscillation frequency. The rapidity of the movement of the probe results in the potential being sampled at two points, V_{P1} and V_{P2} before the electrode noise has changed appreciably. This produces a high sensitivity measurement that is several orders of magnitude more sensitive than is obtained by non-vibrating probe methods.⁵

Ishikawa and Isaacs⁴ at the Brookhaven National Laboratory have adapted the one-dimensional vibrating probe method to study pitting corrosion of aluminum alloys. They have developed a scanning technique whereby the vibrating probe is held in a mechanical stage which is driven by two stepping motors arranged to scan in the X-Y plane parallel to the surface of the specimen. The probe vibrates in the Z direction for measurements of current density normal to the surface of the specimen. By applying a potentiodynamic ramp to the specimen and measuring the current response of the ions streaming from active pits, Ishikawa and Isaacs were able to develop localized polarization curves for pits and surrounding regions.

This study explores the application of the scanning vibrating electrode probe techniques (SVET) to corrosion of welded silicon carbide whisker reinforced 6061 aluminum alloy (SiCw/6061 Al) metal matrix composites (MMC's) and of graphite filament reinforced aluminum (Gr/Al), MMC's.

EXPERIMENTAL

Materials

Three MMC specimens were studied using the scanning vibrating electrode technique (SVET). Two were welded discontinuous SiCw/6061 Al composite specimens. The composite was obtained from ARCO Metals Inc., Greer, South Carolina in the form of 6.35 mm thick rolled plate containing 20 v/o F-9 SiC whisker reinforcement in 6061 aluminum matrix. A micrograph of the composite material is shown in Fig. 2. The plate was provided in a nominal T-6 temper. Weldments were fabricated using methods developed at Martin Marietta Research Labs.⁶ The plate was first degassed in vacuum at 10^{-5} torr at 500°C for 24 hours to remove trapped hydrogen by heat treating prior to welding. Joining was accomplished by gas-metal-arc welding (GMAC) using either 4043 aluminum alloy or 5356 aluminum alloy filler metals to form the joints. Macrographs of these joints showing the parent composite material, the heat affected zone (HAZ), and weld metal are shown in Fig. 3(a & b).

The third specimen was a continuous 40 v/o VSB-32 pitch graphite fiber aluminum composite. The Gr/Al plate was fabricated by DWA Composite Specialities, Inc., Chatsworth, California from liquid metal infiltrated (LMI) wire. The wire was infiltrated with 6061 Al alloy. Plate was fabricated by hot pressing four plies of LMI Gr/Al wire between 0.1 mm face sheets of 1100 Al alloy. The entire composite plate was ~ 2mm thick. Corrosion exposures were performed in 0.6N NaCl electrolyte with the microstructure shown in Fig. 4 exposed to the environment.

Electrochemical Measurements

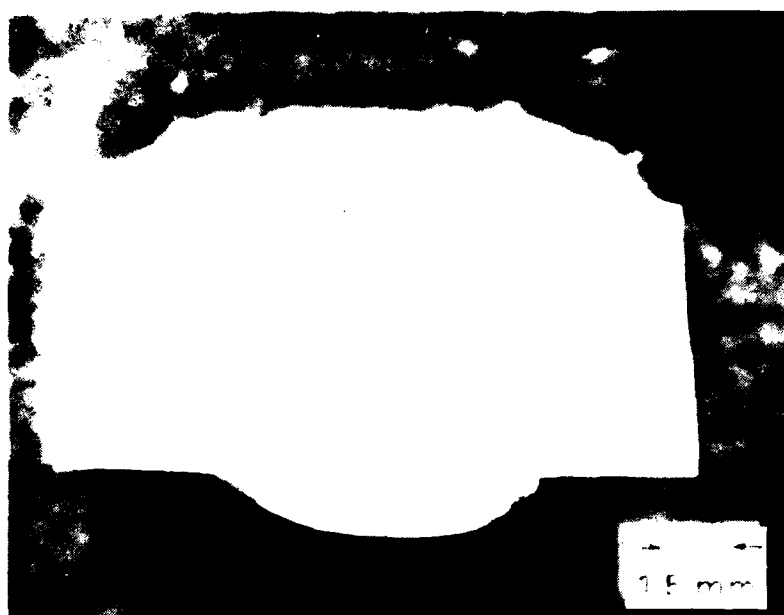
Testing was performed in open cells in laboratory air. All electrochemical measurements were made using 0.6M NaCl electrolytes prepared with reagent grade chemicals and distilled water. The solution resistivity, ρ , was 16 $\Omega \cdot \text{cm}$.

The vibrating probe measurements were performed at the Brookhaven National Laboratory in collaboration with H. Isaacs. The test arrangement consisted of a modified vibrating electrode probe assembly and a probe power supply from the Vibrating Probe Company, Davis, California. A Princeton Applied research Model 5204 lock-in amplifier and Hewlett Packard 9845B mini-computer with a Hewlett Packard 2240 data acquisition system were used to collect and analyze data. Mechanical positioning of the probe in the X-Y plane parallel to the specimen surface was achieved using a stage driven by two stepping motors under HP9845B computer control.

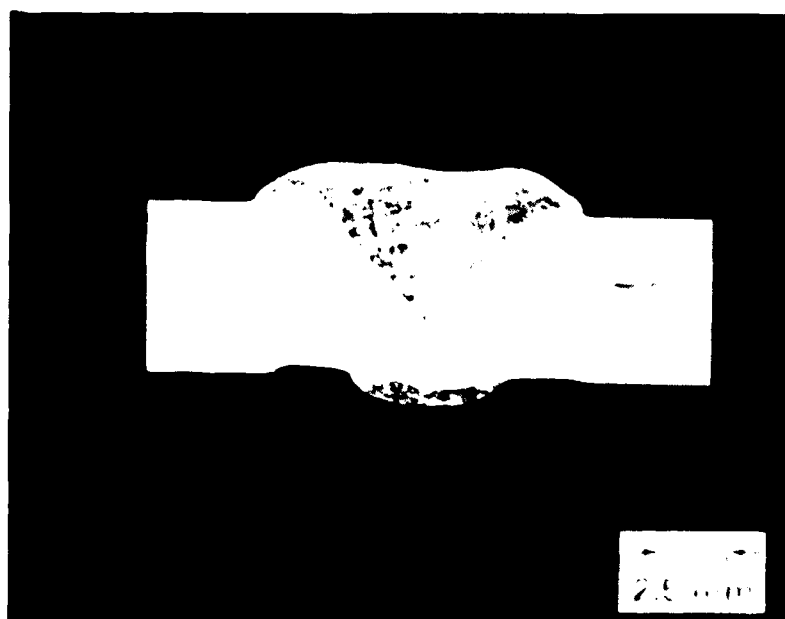
The vibrating probe tip was positioned ~ 0.3 mm above the surface of the composite. The reference electrode was positioned approximately 1 cm above the surface and to the side where no significant current densities were present. The signal from the two electrodes was fed to the differential inputs of the lock-in amplifier and the quadrature was eliminated by adjusting the phase angle to account for the time variation of the vibrating electrode potential. The real component of the vibrating electrode potential was then measured at the extremes of the vibration stroke and the difference in potential was fed to the computer to be processed as a potential gradient. The gradient was then recorded at predetermined grid points and mapped using the



Fig. 2 - Micrograph of 20V/o F-9 SiC/6061-T6 aluminum metal matrix composites



(a)



(b)

Fig. 3 - Macrographs of welded 20V/o F-9 SiC/6061-T6 aluminum metal matrix composite joints: a) Joint formed using 4043 weld metal and b) Joint formed using 5356 weld metal

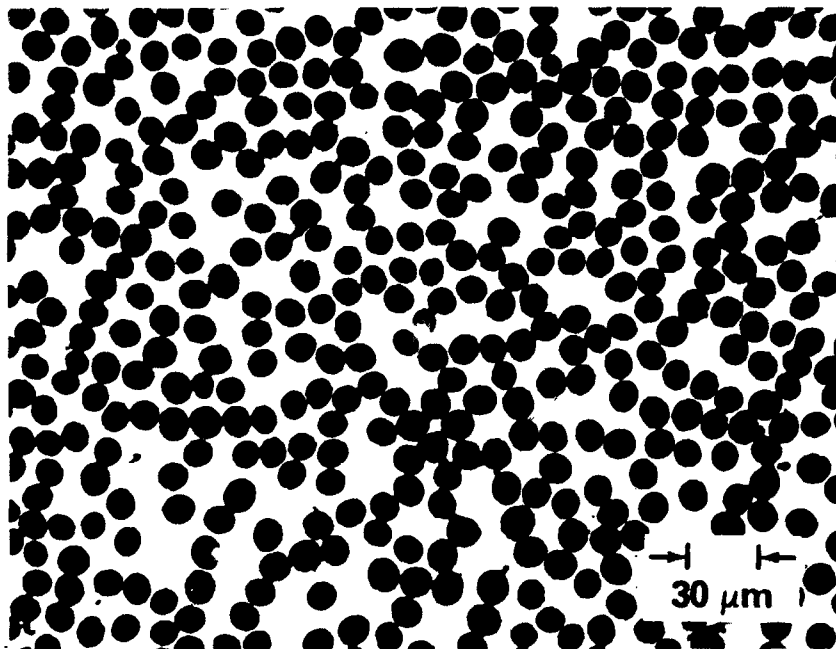


Fig. 4 - Microstructure of liquid metal infiltrated Gr/Al metal matrix composite.

graphics capabilities of the HP9845B. Additional details of the SVET appear in reference.⁴

Scanning Electron Microscopy

Scanning electron microscopy (SEM) was performed in a Coates and Welter Quicksan SEM. The specimens were cleaned in alcohol to remove corrosion products, but were not coated prior to viewing in the SEM.

RESULTS AND DISCUSSION

Contour maps of the local ionic currents normal to the corroding SiC_w/Al welded with 4043 aluminum alloy and welded with 5356 aluminum alloy are shown in Fig.'s 5 a) & b) respectively. In both figures, the region of highest corrosion current density is shown shaded. Open circuit corrosion potentials of these samples were -0.723 volts vs. SCE and -0.765 volts vs. SCE for the 4043 and for the 5356 containing specimens, respectively. Cross sections of these contour maps in the X direction at Y = 2500 μm for the SiC/Al-4043 specimen and at Y = 3500 μm for the SiC/Al-5356 specimen are shown in Fig.'s 6 a) and b), respectively. The location of the HAZ relative to the weld metal and the parent MMC is indicated in the figures.

Comparison of Fig.'s 5 a) and b) with the corresponding macrographs of Fig.'s 3 a) and b) shows the region of highest corrosion is roughly associated with the location of the HAZ and edge effects. This is to be expected since Ahearn and Cook have shown that the HAZ contains Al₄C₃ produced during welding.⁶ Al₄C₃ reacts with water to form methane⁷ according to:

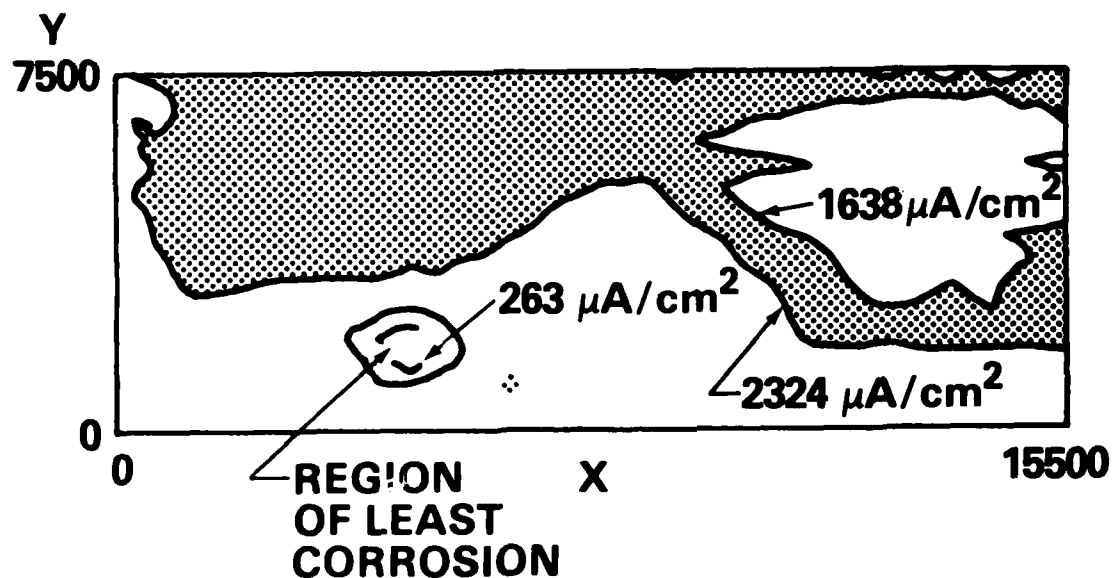
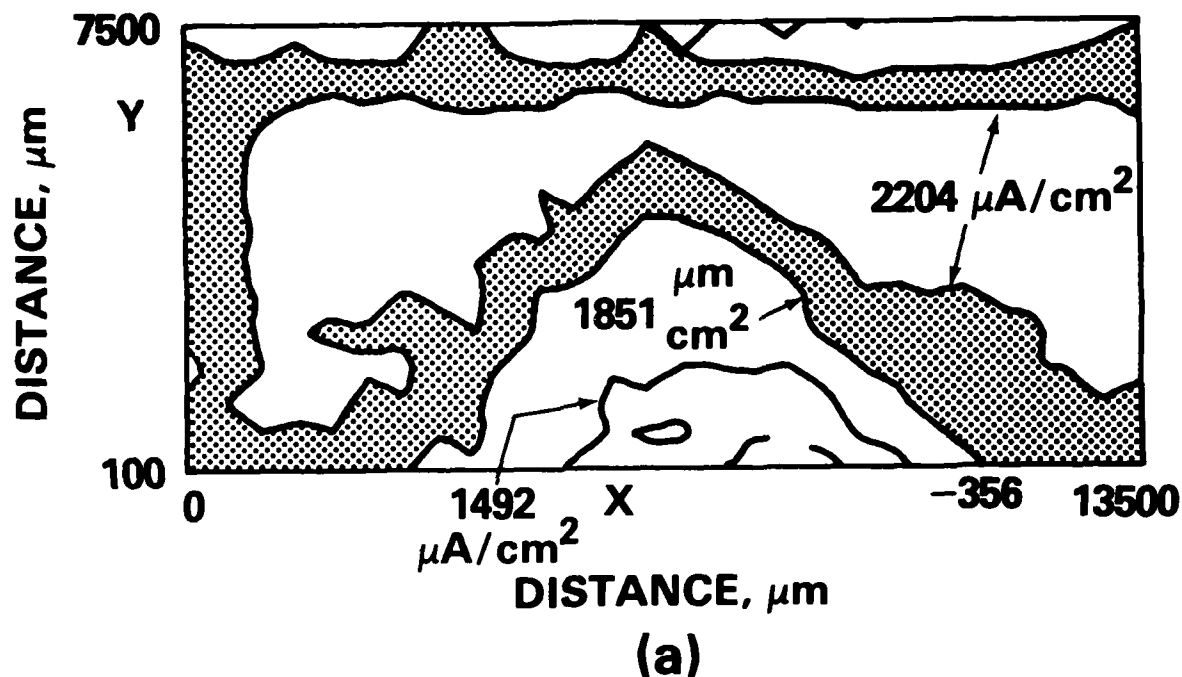
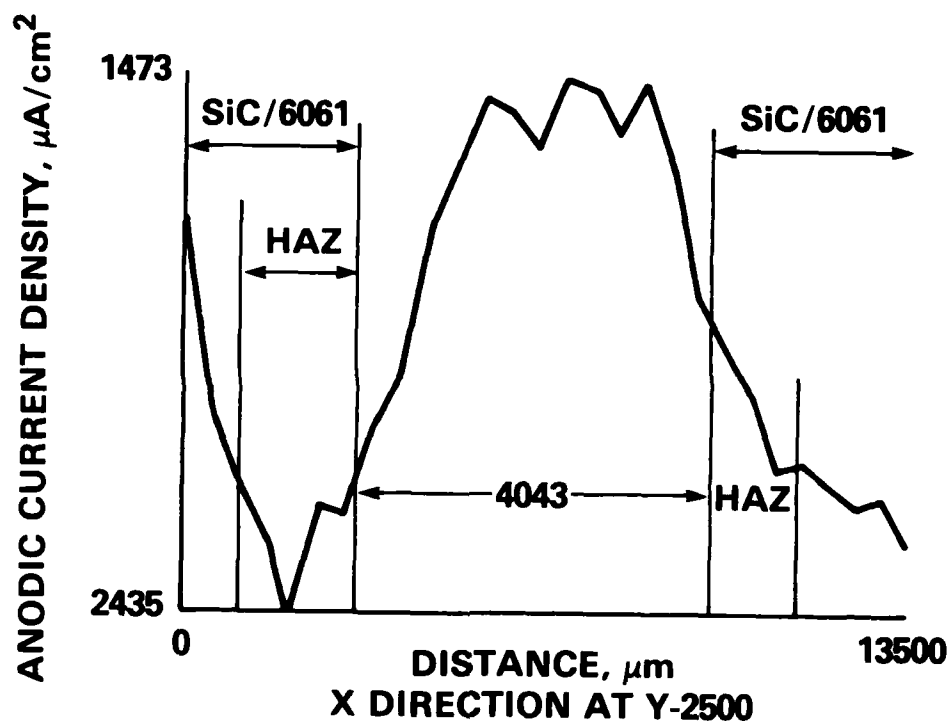
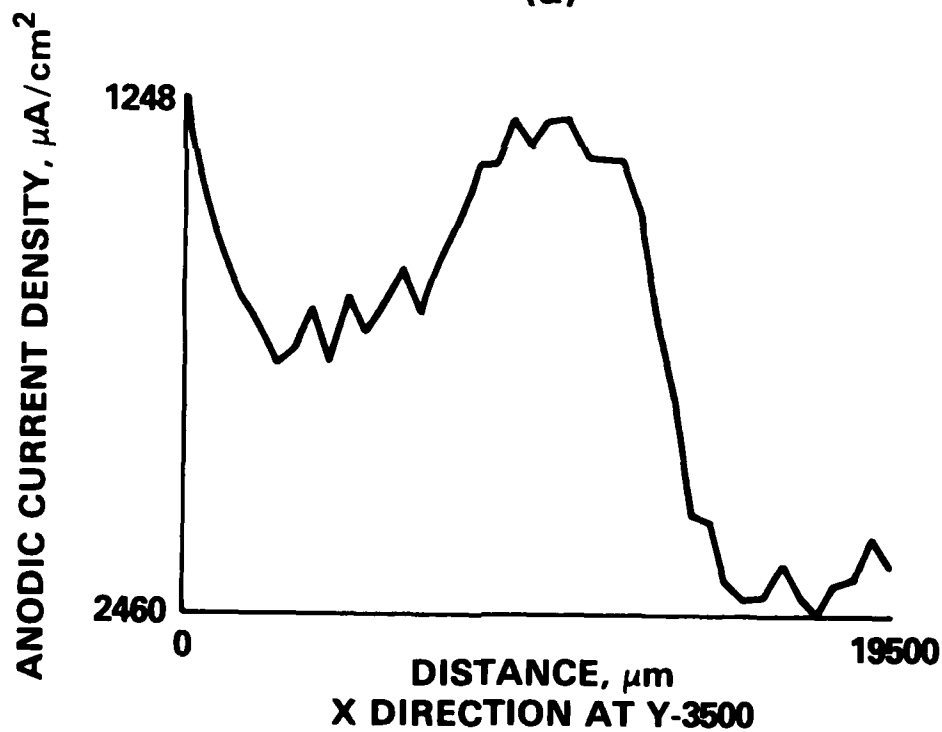


Fig. 5 - Contour maps of normal ionic current flow in welded 20V/o F-9 SiC/6061-T6 metal matrix composites: a) Using 4043 aluminum weld metal and b) Using 5356 aluminum weld metal. Shaded regions are regions of highest corrosion rate. Contour lines are in $\mu\text{A}/\text{cm}^2$.

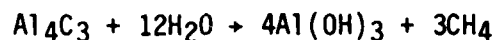


(a)



(b)

Fig. 6 - Cross sections from the current density contour maps: a) in X direction at $\gamma = 2500 \mu\text{m}$ on SiC/Al with 4043 Al weldment and b) in X direction at $\gamma = 3500 \mu\text{m}$ on SiC/Al with 5356 Al weldment



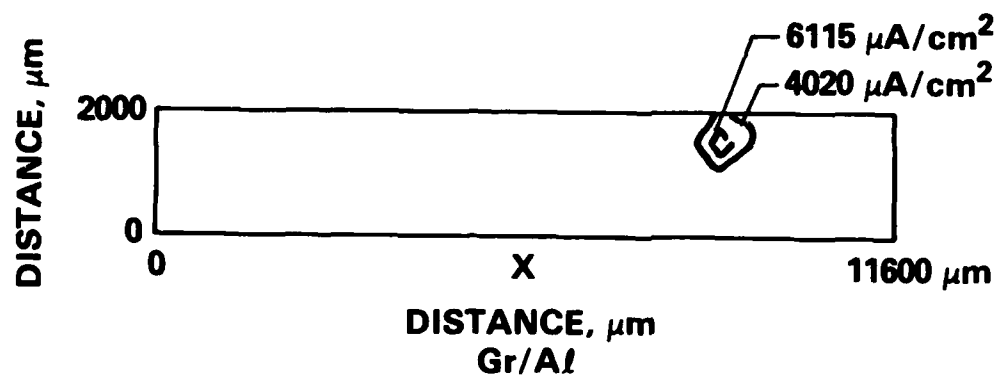
This reaction, along with other metallurgical variations caused by the heat of welding, leads to increased degradation of the HAZ relative to surrounding areas.

It is perhaps significant to note that no enhanced corrosion due to crevice corrosion in the welded specimens appeared in the contour maps.

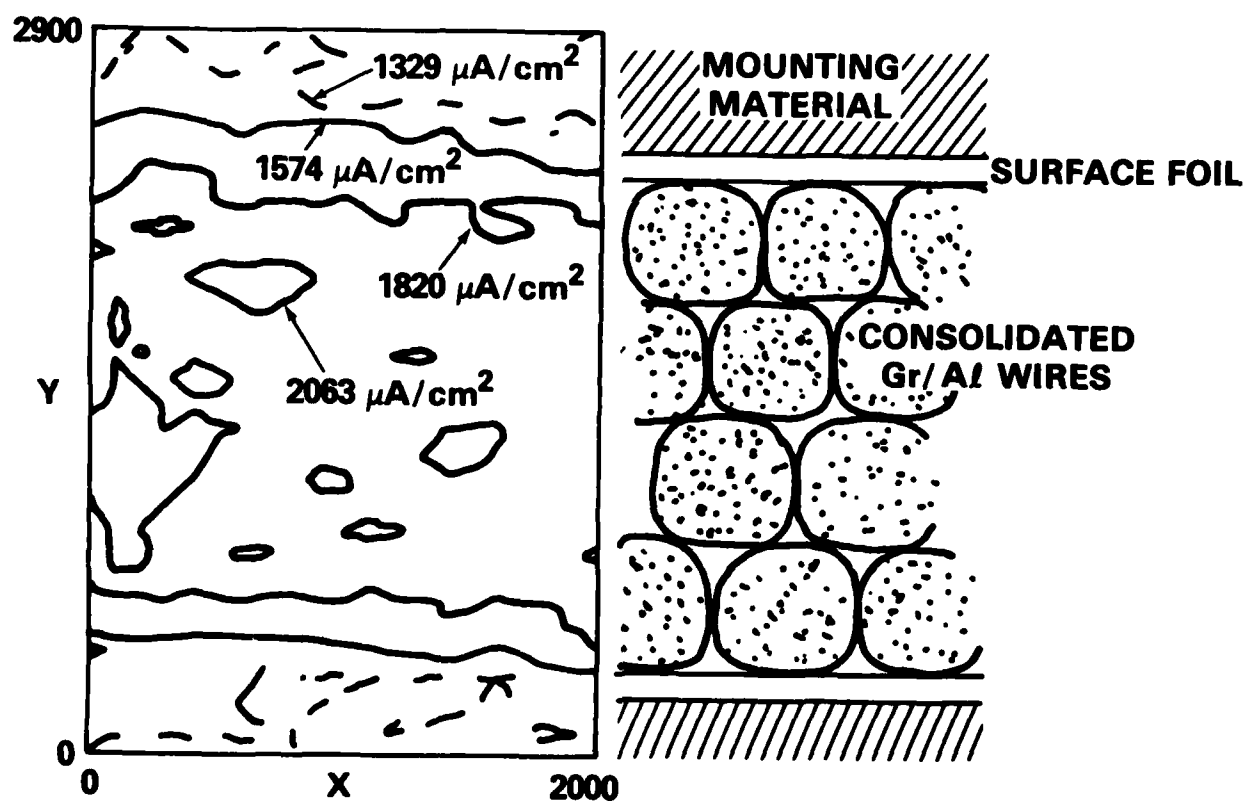
Contour maps of the local normal ionic current of the Gr/Al specimen are shown in Fig. 7. The open circuit corrosion potential of this specimen was -0.705 volts vs. SCE. Attention is immediately drawn to the region of high current density in the upper right hand sector of the specimen (Fig. 7 a). This region of high corrosion activity is associated with the flaws shown in the SEM micrographs of Fig.'s 8 a), b), and c). A small pit (A) and an uninfiltrated region (B) are connected by a crack to form the flaw. The true current density at the flaw is higher than that shown in Fig. 7 a) due to field fall-off at the position of the measurement from the source. Since the flaw is very deep, conditions for the formation of active localized corrosion are immediately present. Although the exact details of the corrosion reactions in the flaws are not known, it is expected that the ionic current streaming from the flaw results from a combination of Al^{+3} , $\text{Al}(\text{OH})^{+2}$, and H^+ ion migration. No gas was observed evolving from the flaw even though H_2 and CH_3 gaseous products might be expected. In other specimens, however, gas evolution from flaws has been observed.

Rapid degradation of Gr/Al composites caused by flaws of the type shown in Fig.'s 8 a), b), and c) have been observed in a number of studies.⁸⁻¹² The general observations are that corrosion proceeds preferentially at wire-foil, foil-foil, and wire-wire interfaces causing separation and yielding $\text{Al}_2\text{O}_3 \cdot 3\text{H}_2\text{O}$ corrosion product. The degradation process, once initiated, proceeds rapidly by exfoliation causing disintegration of the composite. Disintegration may be accelerated by corrosion product wedging at the flaw. The normal corrosion reaction in an open configuration yields, through a series of steps, $\text{Al}(\text{OH})_3$ corrosion product. The $\text{Al}(\text{OH})_3$ when freshly formed, is gelatinous but becomes a white gritty hydrated Bayerite $\text{Al}_2\text{O}_3 \cdot 3\text{H}_2\text{O}$ on aging. This corrosion product is observed in copious quantities on exfoliated sheets. Al_4C_3 formed during consolidation at the graphite/aluminum interface may also be important since the $\text{Al}_4\text{C}_3\text{-H}_2\text{O}$ reaction also produces $\text{Al}(\text{OH})_3$. The process is exacerbated by the low transverse strengths (typically 20 MPa) in these materials. Figures 8 a), b), and c) are consistent with the early stages of this mechanism. The crack is thought to be a result of corrosion product wedging at the pit and at the uninfiltrated region. It was not present on the sample prior to exposure to the corrodent.

The role of corrosion product wedging in the early stages of the degradation process is, however, not clear. In the confined space of the flaw in the presence of chlorides, the primary corrosion reaction and the $\text{Al}_4\text{C}_3\text{-H}_2\text{O}$ reaction may not produce $\text{Al}(\text{OH})_3$. This is because the pH decreases in crevices in aluminum alloys due to hydrolysis of corrosion products. This decrease of pH would likely retard $\text{Al}(\text{OH})_3$ formation, since the solubility of this compound increases rapidly at pH ~ 5 . The hydrolysis reaction in the crevice would produce an electrolyte in the flaw with a pH that was dependent

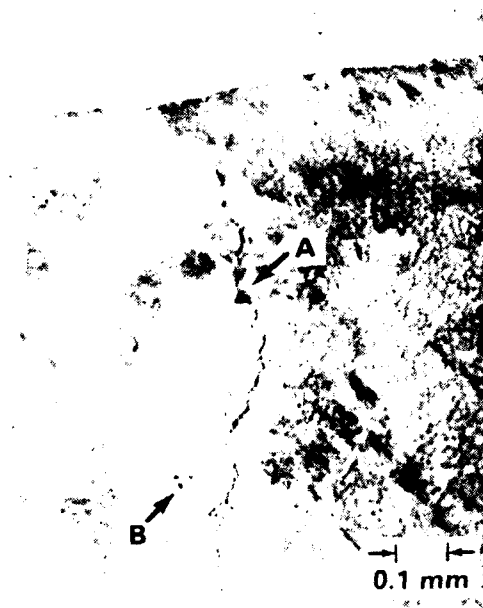


(a)



(b)

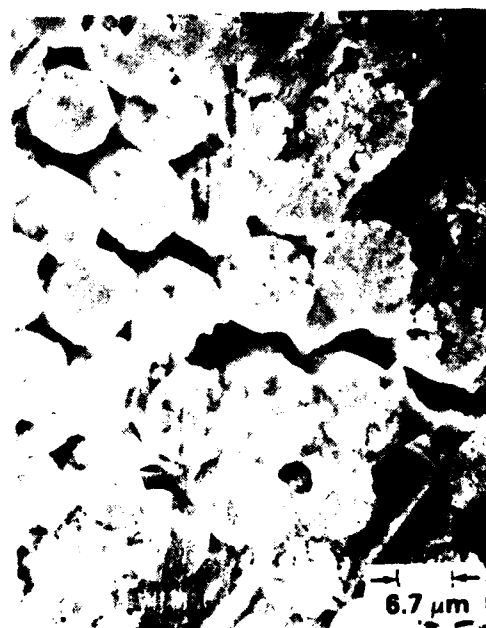
Fig. 7 - Ionic current density maps from Gr/Al MMC: a) overall view showing current from flaw and b) local view away from flaw



(a)



(b)



(c)

Fig. 8 - Microstructures of Gr/Al at flaw region: a) overall view, b) at pit, and c) at unfiltered region

on flaw geometry (i.e. depth and width). At the flaw base, the pH would be in the 3.5 range, increasing to the bulk value of 6.5 outside the flaw. Corrosion product wedging would occur when the local chemistry permitted voluminous solid corrosion products to form in the flaw cavity.

Another complicating factor is that the matrix material may have a propensity to exfoliate because of intermetallic compound formation in the matrix material during fabrication. Intermetallic particles containing manganese, copper, iron, and aluminum, are known to act as efficient cathodic sites along anodic corrosion paths and can lead to exfoliation in 6061 Al when the intermetallics are present in an appropriate morphology.

A contour map away from the flaw is shown in Fig. 7 b). Again, the pattern is consistent with the microstructure of Fig 4. Galvanic effects associated with the 1100 aluminum surface, the 6061 aluminum alloy matrix, and the regions of high graphite content are readily distinguished. An SEM micrograph of the corroded surface, Fig. 9, shows corrosion of the aluminum; however, degradation in these well bonded areas is much less severe. Comparison of the magnitude of the currents from the flawed region and the well bonded region shows that the corrosion rate of the latter region is at least a factor of 3 less than the rate near the flaw.

It is interesting to note that net ionic currents flowing into the specimen (cathodic currents) were not detected in any of the regions of the composite. This is consistent with the cathodic reaction being the reduction of O_2 at cathodic sites. The measured open circuit potential of -0.705 volts vs. SCE falls close to the reversible electrode potential of the graphite, indicating that the graphite electrodes are not polarized. This also indicates that the active galvanic couple is the Al/ O_2 couple as would be expected in this system. The graphite most likely acts as sites for the oxygen reduction reaction.

There are several limitations to the vibrating probe technique which should be discussed. First, the spatial resolution of the SVET is marginal in resolving localized corrosion in well bonded Gr/Al. It is, however, more than adequate in detecting corrosion activity at flaws. Secondly, in order to obtain quantitative current density at the surface of the sample, an extrapolation procedure to account for field fall-off from the central point of measurement to the surface is necessary. The procedure for this extrapolation is not straightforward because the extrapolation function is dependent upon the source strength and the location of the anodes and cathodes on the sample surface. In the simple case of a single point current source (i.e., a small diameter pit) the current falls off as the inverse square of the distance. If the current source is an embedded disk, the current falls off exponentially with the distance. In the general case, the extrapolation function depends on the location, size, and potential of the anodes and cathodes. It is, therefore, unlikely that analytical or finite element solutions to obtain extrapolation functions will be readily available. Thus an experimental measure to obtain an extrapolation function is required to obtain quantitative values for the current density at the specimen surface.

Another major limitation of the 1-D vibrating probe technique is that only the component of the current parallel to the line of oscillation is measured. The orientation of this line relative to the surface must be

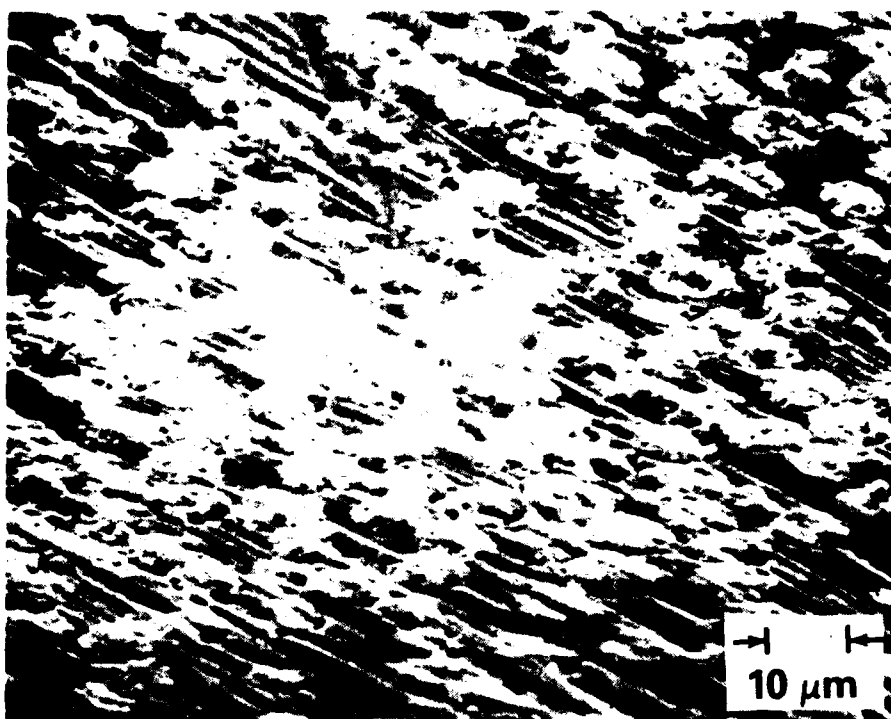


Fig. 9 - SEM micrograph of corroded Gr/Al in region where fiber and matrix are well bonded.

accurately known to obtain an accurate one component measurement. In general, ionic current flow in the electrolyte is governed by the three dimensional law of conservation of charge. In differential equation form this law can be stated as

$$\nabla \cdot \bar{J} = -\partial \rho / \partial t \quad (2)$$

where \bar{J} is the current density, ρ is the charge density, and t is time. The constitutive relationship (Ohm's Law) between current density and the

electric field intensity, \bar{E} , in terms of the electrical conductance, σ , is

$$\bar{J} = \sigma \bar{E} \quad (3)$$

where, by definition, the electric field intensity is given by

$$\bar{E} = -\nabla \phi \quad (4)$$

and ϕ is the electrical potential.

Substituting equations (3) and (4) into (2) yields

$$\nabla \cdot \sigma \nabla \phi = -\frac{\partial \rho}{\partial t} \quad (5)$$

Therefore, a three-dimensional spatial representation of the ionic current and the local value of the electrolyte conductivity is needed to obtain a general characterization of the corrosion cell. Since Jaffe's probe is one dimensional, it is necessary to change the relative orientation of the probe and the sample to obtain the other two orthogonal components of the ionic current. Experimentally, this is difficult to accomplish, time consuming, and leads to uncertainties regarding the location of the current measurement. It can lead to errors if the magnitude or direction of the current is changing with time. The method also does not measure the local value of the pH or the local electrolyte conductivity so bulk measurements must be used.

CONCLUSIONS

Scanning vibration electrode techniques (SVET) provide a useful method to obtain a qualitative description of localized corrosion in composite materials where the scale of the microstructure matches the spatial resolution of the SVET. The relative severity of pits and crevices is discernible as are spatial variations of the ionic currents associated with the corrosion process.

The observations demonstrate that corrosion effects from metallurgical variations due to welding of SiC/Al can be detected and areas of accelerated corrosion activity delineated. The observations of the corroding Gr/Al specimen imply that the corrosion rate of the composite in the absence of flaws would depend upon the catalytic properties of the graphite in promoting or retarding the oxygen reduction reaction as well as the rate of diffusion of O_2 to the surface. Both the exchange current density for the reaction and the Tafel constant would affect the oxygen reduction reaction rate. Thus, the corrosion rate in the absence of flaws might be improved by additions of poisons to the fiber to retard the oxygen reduction reaction on graphite. The fact that an increase in the anodic current streaming from the flaws was detected indicates that interface and crevice corrosion is important. Al_4C_3 formation at the Gr/Al interfaces and also the crevice corrosion characteristics of the aluminum matrix alloy may affect the degradation rate of the Gr/Al due to the exfoliation process. Selection of alloys for composite fabrication which are less susceptible to crevice corrosion and to Al_4C_3 formation during consolidation of the composite are likely to produce decreased degradation rates. Improvements in transverse strength should also reduce exfoliation.

Advances in the state-of-the-art of SVET would be achieved with the development of 3-D vibrating probes.

ACKNOWLEDGMENTS

The author would like to express his appreciation to Dr. Hugh Isaacs of the Brookhaven National Laboratory for the use of the scanning vibrating probe and his invaluable assistance and consultation in performing the electrochemical measurements.

Funding for this work was provided by the Office of Naval Research and by the Defense Advance Research Projects Agency.

REFERENCES

1. L.F. Jaffee and R. Nuccitelli, J. Cell Biology, 63, 614 (1974).
2. J.A. Freeman and J.P. Wikswo, Biophysical J., 37, 79A (1982).
3. J.A. Freeman, B. Mayes, G.J. Snipes, and J.P. Wikswo, Society for Neuroscience, in press.
4. Y. Ishikawa and H.S. Isaacs, Brookhaven National Lab, "Study of Pitting Corrosion of Aluminum by Means of the Scanning Vibrating Probe Electrode Technique" Report BNL 33059, 1983, (AD-D129610).
5. L.J. Gainer and G.R. Wallwork, Corr., 35, 61 (1979).
6. J.S. Ahearn and D.C. Cooke, Martin Marietta Laboratories, "The Weldability of SiC/Al Metal Matrix Composites" Report MML TR 82-15C, 1982, (AD-B067578L).
7. C.A. Jacobson, Encyclopedia of Chemical Reactions, (Reinhold:New York: 1946).
8. L.W. Davis and P.G. Sullivan, "Evaluation of Gr/Al Composite Materials"; Contract N00017-73-C-4313, Quarterly reports 1-4, Naval Ordnance Systems Command, Washington, D.C. 1973.
9. D.L. Dull, W.C. Harrigan, and M.F. Amateau, "The Effect of Metal Matrix Composites on Mechanical Strength and Corrosion Behavior of Graphite-Aluminum Composites" Aerospace Corp., Report No. ATR-76 (7564)-1, 1977.
10. D.L. Dull, W.C. Harrigan, and M.F. Amateau, "The Corrosion of 6061 Aluminum Alloy Thornel 50 Graphite Composites in Distilled Water and NaCl Solution" Aerospace Corp., Report No. TR-0075 (5621)-2, 1975, AD-A011761.
11. J.H. Payer and W.H. Pfeifer, "A Review of the Status of the Battelle Corrosion Studies on Graphite Fiber Reinforced Aluminum Alloy Composites" presented at Launch Vehicles Materials Workshop, Daytona Beach, Florida, Feb. 1975.
12. W.H. Pfeifer in Hybrid and Select Metal-Matrix Composites, W.J. Renton, ed. (AIAA:New York:1977), p. 159.
13. V.P. Batrokov, V.S. Komissarova, and N.V. Egorava, Metalloved. Term. Obrab. Met., 10, 52 (1978).
14. K.I. Portnoi, N.I. Timofeeva, A.A. Zabolotskii, V.N. Sakovich, B.F. Trefilov, M. Kh. Levinskaya, and N.N. Polyak, Poroshkovaya Metallurgiya, 218, 45 (1981).

END

FILMED

4-85

DTIC